Available at
http://pvamu.edu/aam
Appl. Appl. Math.
ISSN: 1932-9466

Vol. 6, Issue 1 (June 2011) pp. 27 – 40
(Previously, Vol. 6, Issue 11, pp. 1767 – 1780)

Applications and Applied Mathematics:
An International Journal
(AAM)

On Temporal Instability of Electrically Forced Axisymmetric Jets with Variable Applied Field and Nonzero Basic State Velocity

Dambaru Bhatta, Sayantan Das and Daniel N. Riahi

Department of Mathematics
The University of Texas-Pan American
Edinburg, Texas 78539-2999 USA
bhattad@utpa.edu, sdas@broncs.utpa.edu, Riahid@aol.com

Received: June 28, 2010; Accepted: February 18, 2011

Abstract

The problem of instability of electrically forced axisymmetric jets with respect to temporally growing disturbances is investigated computationally. We derive a dispersion relation based on the relevant approximated versions of the equations of the electro-hydrodynamics for an electrically forced jet flow. For temporal instability, we find in the realistic cases of the non-zero basic state velocity that the growth rate of the unstable mode is unaffected by the value of the basic state velocity. However, the non-zero value of the basic state velocity affects significantly the period of the unstable mode in the sense that it decreases the period, and the rate of increase of the frequency with respect to the axial wave number increases with the basic state velocity. It is also observed from numerical investigations that there are two modes of instability for small values of the wavenumber.

Keywords: Axisymmetric, electrospinning, electric field, jet flow, temporal instability

MSC 2010 No.: 35Q35, 35Q60

1. Introduction

Our main contribution to the present work has been to implement a numerical procedure to determine computational results about the effects of non-zero basic flow velocity in

the electrically driven jet flow system. Temporal instability of a cylindrical jet of fluid with a static charge density in the presence of an external constant as well as variable electric field is considered in this paper. The investigation of electrically forced jets is gaining importance in applications such as those of electrospraying Baily (1988) and electrospinning Hohman et al. (2001a, 2001b). Electrospraying uses electric field to produce and control sprays of very small drops that are uniform in size. Electrospinning process uses electric fields to produce and control thin, uniform, high quality fibers. In the absence of electrical effects, it had been observed that temporal growing disturbances can destabilize the free shear flows which include the jet flows Drazin and Reid (1981). Since then several authors Hohman et al. (2001a, 2001b), Saville (1971), Reneker et al. (2000), Shkadov and Shutov (2001) and Fridrikh et al. (2003) have done theoretical studies on temporal instability of the electrically forced jets in the presence of electrical effects. Hohman et al. (2001a, 2001b) developed a theoretical understanding of temporal instabilities for an electrically forced jet with a static charge density. The equations for the dependent variables of the disturbances were based on the long wavelength and asymptotic approximations of the governing electro-hydrodynamic equations. They found that the dominance of the instabilities depends on the surface charge density and the radius of the jet.

Saville (1971) studied interactions between electrical tractions at the interface of an electrically driven liquid jet and the linear temporal instability phenomena. It was found, in particular, that when viscous effects are small, sufficiently small strength of the electric fields tends to decrease the growth rate of a temporally growing axisymmetric mode. However, when viscous effects predominate, then the only unstable disturbance is that due to the axisymmetric mode regardless of the magnitude of the field's strength. Other investigations of electrically driven jets with applications in electrospinning of nanofiber are reported in Yarin et al. (2001), Sun et al. (2003), Li and Xia (2004) and Yu et al. (2004). Spatial instability of axisymmetric electrically forced jets with variable applied field under idealistic conditions of zero or infinite electrical conductivity was studied analytically by Riahi (2009). He reported two spatial modes of instability each of which was enhanced with increasing the strength of the externally applied electric field.

In this paper, we follow an approach similar to that of Hohman et al. (2001a) to obtain a mathematical model for the electrically driven jets. We consider the problem of instability of electrically forced axisymmetric jets with respect to temporally growing disturbances. We derive a dispersion relation based on the relevant approximated versions of the equations of the electro-hydrodynamics for an electrically forced jet flow. The approximations include the assumptions that the length scale along the axial direction of the jet is much larger than that in the radial direction of the jet and the disturbances are axisymmetric and infinitesimal in amplitude. Indeed it is an extension of the work of Homan et al. (2001a) in the sense that our model also incorporates non-zero basic velocity and non-zero surface charge density. We then determine the dispersion relation, between the growth rate of the spatially growing disturbances and the wave number in the axial direction, the frequency and the non-dimensional parameters of the model. We found a number of interesting results. In particular, the growth rate of the temporally growing disturbances is found to be independent of the basic state velocity, while the frequency and equivalently the period of the growing disturbances are found to depend notably on the basic state velocity. It is also observed from numerical investigations that there are two modes of instability for small values of the wavenumber.

2. Formulation

The present theoretical investigation for the mathematical modeling of the electrically driven jets is based on the original governing electro-hydrodynamic equations Melcher and Taylor (1969) for the mass conservation, momentum, charge conservation and the electric potential. The system is given by

$$\frac{D\rho}{Dt} + \rho\nabla\cdot\vec{u} = 0, \tag{1a}$$

$$\rho\frac{D\vec{u}}{Dt} = -\nabla P + \nabla\cdot\nabla\left(\mu\vec{u}\right) + q\vec{E}, \tag{1b}$$

$$\frac{Dq}{Dt} + \nabla\cdot\left(K\vec{E}\right) = 0, \tag{1c}$$

and

$$\vec{E} = -\nabla\Phi\,, \tag{1d}$$

where $\frac{D}{Dt} = \frac{\partial}{\partial t} + \vec{u}\cdot\nabla$ is the total derivative with is used to denote dot product. Here $\vec{u}$ is the velocity vector, P is the pressure, $\vec{E}$ is the electric field vector, Φ is the electric potential, q is the free charge density, ρ is the fluid density, μ is the dynamic viscosity, K is electric conductivity and t is the time variable. The geometry we use is shown in Figure 1.

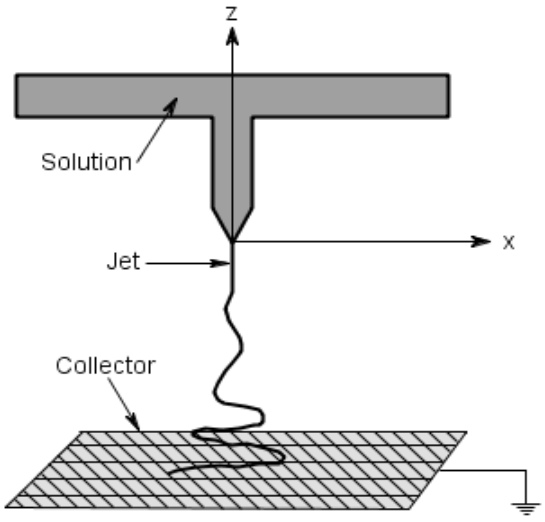

Figure 1. Electrospinning model

The internal pressure in the jet can be found by taking into consideration the balances across the free boundary of the jet between the pressure, viscous forces, capillary forces and the electric

energy density plus the radial self-repulsion of the free charges on the free boundary Melcher and Taylor (1969). Assuming the ambient air to be motionless and passive, this yield the following expression for the pressure P in the jet

$$P = \gamma\kappa - \left[(\varepsilon - \widetilde{\varepsilon})/8\pi\right]E^2 - \left(4\pi/\widetilde{\varepsilon}\right)\sigma_0/\widetilde{\varepsilon}\,, \tag{2}$$

where γ is the surface tension, κ is twice the mean curvature of the interface, $\varepsilon/(4\pi)$ is the permittivity constant in the jet, $\widetilde{\varepsilon}/(4\pi)$ is the permittivity constant in the air and σ is the surface free charge.

Following the previous investigation Hohman et al. (2001a), we consider a cylindrical fluid jet moving axially. The fluid of air is considered as the external fluid, and the internal fluid of jet is assumed to be Newtonian and incompressible. We use the governing equations (1) in the cylindrical coordinate system with origin at the center of nozzle exit section, where the jet flow is emitted with axial z-axis along the axis of the jet. We consider the axisymmetric form of the dependent variables in the sense that the azimuthal velocity is zero and there are no variations of the dependent variables with respect to the azimuthal variable. Following approximations carried out in Hohman et al. (2001a) for a long and slender jet in the axial direction, we consider length scale in the axial direction to be large in comparison to that in the radial direction and use a perturbation expansion in the small jet' aspect ratio.

We expand the dependent variables in a Taylor series in the radial variable *r*. Then such expansions are used in the full axisymmetric system and keep only the leading terms. These lead to relatively simple equations for the dependent variables as functions of t and z only. Following the method of approach in Hohman et al. (2001a), we employ (1d) and Coulomb's integral equation to arrive at an equation for the electric field, which is essentially as the one derived by Hohman et al. (2001a) and will not be repeated here. Equations presented in (1) are the general governing equations applicable to general cases for electrically forced jet systems, and for this generality aspect no boundary conditions in needed to be provided. Equations described by (3) are simple modeling one dimensional linear equations admitting periodic solutions for perturbations in the axial direction. As is known from experimental and theoretical work by Hohman et al. (2001a, 2001b), such periodic form in axial direction is reasonable, provided the axial domain should be away from the jet inlet section, which is assumed in our paper.

We non-dimensionalize the resulting equations using r_0 (radius of the cross sectional area of the nozzle exit at z=0), $E_0 = \sqrt{\dfrac{\gamma}{(\varepsilon - \widetilde{\varepsilon})r_0}}$, $t_0 = \sqrt{\dfrac{\rho r_0}{\gamma}}$, $\dfrac{r_0}{t_0}$ and $\sqrt{\dfrac{\gamma\widetilde{\varepsilon}}{r_0}}$ as scales for length, electric field, time, velocity and surface charge, respectively. The resulting non-dimensional equations are then

$$\frac{\partial}{\partial t}\left(h^2\right) + \frac{\partial}{\partial z}\left(h^2 v\right) = 0, \tag{3a}$$

$$\frac{\partial}{\partial t}\left(h\sigma\right) + \frac{\partial}{\partial z}\left(hv\varsigma\right) + \frac{1}{2}\frac{\partial}{\partial z}\left(h^2 EK\right) = 0, \tag{3b}$$

$$\frac{\partial v}{\partial t}+v\frac{\partial v}{\partial z}=-\frac{\partial}{\partial z}\left[\frac{h}{\sqrt{1+\left(\frac{\partial h}{\partial z}\right)^2}}-\frac{\frac{\partial^2 h}{\partial z^2}}{\sqrt[3]{1+\left(\frac{\partial h}{\partial z}\right)^2}}-\frac{E^2}{8\pi}-4\pi\sigma^2\right] + \frac{2E\sigma}{h\sqrt{\beta}}+\frac{3\nu^*}{h^2}\frac{\partial}{\partial z}\left(h^2\frac{\partial v}{\partial z}\right), \tag{3c}$$

and

$$E_b(z)=E-\ln(\chi)\left[\frac{\beta}{2}\frac{\partial^2}{\partial z^2}\left(h^2E\right)-4\pi\sqrt{\beta}\frac{\partial}{\partial z}\left(h\sigma\right)\right], \tag{3d}$$

where v is the axial velocity, $h(z, t)$ is the radius of the jet' cross-section at the axial location z, $\sigma(z, t)$ is the surface charge, $E(z, t)$ is the electric field, the conductivity K is assumed to be a function of z in the form $K = K_0\tilde{K}(z)$, where K_0 is a constant dimensional conductivity and $\tilde{K}(z)$ is a non-dimensional variable function. Also, non-dimensional conductivity is given by $K^*=K_0\sqrt{\frac{\rho r_0^{\,3}}{\gamma\beta\tilde{\varepsilon}^2}}$ and $\beta=\frac{\varepsilon}{\tilde{\varepsilon}}-1$. Also $\nu^*=\sqrt{\frac{\nu_0^{\,2}\rho r_0}{\gamma}}$ is the non-dimensional viscosity parameter, $E_b(z)$ is an applied electric field and $\frac{1}{\chi}$. is the local aspect ratio, which is assumed to be small. Next, we determine the electrostatic equilibrium solution, which is referred to here as the basic state solution, to the equations (3a-3d). The basic state solutions for the dependent variables, which are designated with a subscript 'b', are given below

$$h_b=1,\quad v_b=v_0,\quad \sigma_b=\sigma_0,\quad E_b=\Omega_0(1\text{-}\delta z), \tag{4a-d}$$

where both v_0, σ_0 and Ω_0 are constant quantities, and $\delta = 8\sigma_0\pi/(\Omega\sqrt{\beta})$ is assumed to be a small parameter ($\delta << 1$), under which the basic state solutions given by (4a-d) were found to satisfy the modeling equations Riahi (2009). δ represents a composite parameter proportional to the basic state surface charge. It is assumed that δ is sufficiently small so that to leading terms eqns (3) do not contain z-dependent coefficients and so the present method of approach can be implemented. Here, σ_0 is referred to as the background free charge density. We consider each dependent variable as sum of its basic state solution plus a small perturbation, which is assumed to be oscillatory in time and in axial variable. Thus, we write

$$\left(h, v, \sigma, E\right)=\left(h_b, v_b, \sigma_b, E_b\right)+\left(h_1, v_1, \sigma_1, E_1\right), \tag{5a}$$

where the perturbation quantities, designated by the subscript '1', are given by

$$\left(h_1, v_1, \sigma_1, E_1\right) = \left(\tilde{h}, \tilde{v}, \tilde{\sigma}, \tilde{E}\right) e^{\omega t + ikz}. \tag{5b}$$

Here, $\left(\tilde{h}, \tilde{v}, \tilde{\sigma}, \tilde{E}\right)$ are constants which are assumed to be small, i is the imaginary unit, ω is the complex growth rate, and k is the axial wave number. We need four equations for the variables: $\tilde{h}, \tilde{v}, \tilde{\sigma}, \tilde{E}$. Using (4)-(5) in (3), we linearize with respect to the amplitude of perturbation, consider a series expansion in powers of δ for all the dependent variable and only retain the lowest leading order terms, and then divide each equation by the exponential function exp [$\omega t+ikz$]. We then obtain 4 linear algebraic equations for the unknown constants $\left(\tilde{h}, \tilde{v}, \tilde{\sigma}, \tilde{E}\right)$. To obtain non-trivial (non-zero) values of these constants, the 4x4 determinant of the coefficients of these unknowns must be zero, which yields the following dispersion relation:

$$\omega^3 + T_1\omega^2 + T_2\omega + T_3 = 0 \tag{6}$$

where

$$T_1 = 3k\left(\nu^* k + i v_b\right) + \frac{4\pi K^* \Lambda}{D\sqrt{\beta}} \tag{7}$$

$$T_2 = k^2\left[\frac{k^2-1}{2} + \frac{12\pi\nu^* K^* \Lambda}{D\sqrt{\beta}} + 4\pi\sigma_b^2\left(\frac{4\Gamma}{D} - 1\right) + \frac{E_b^2 \Lambda}{4\pi D} + i v_b\left(3 i v_b + 6k\nu^* + \frac{8\pi K^* \Lambda}{kD\sqrt{\beta}}\right)\right] \tag{8}$$

$$T_3 = \frac{4\pi k^2 K^* \Lambda}{D\sqrt{\beta}}\left[\frac{k^2-1}{2} + \frac{E_b^2 D}{4\pi\Lambda} + 4\pi\sigma_b^2 + \frac{2i\sigma_b E_b}{k\sqrt{\beta}}\left(\frac{1}{\Gamma} - 2\right)\right] + i k^3 v_b\left[\frac{k^2-1}{2} + \frac{E_b^2 \Lambda}{4\pi D} + 4\pi\sigma_b^2\left(\frac{4\Gamma}{D} - 1\right) + \frac{12\pi\nu^* K^* \Lambda}{D\sqrt{\beta}}\right] - k^2 v_b^2\left[3\nu^* k^2 + \frac{4\pi K^* \Lambda}{D\sqrt{\beta}} + i k v_b\right] \tag{9}$$

with

$$\chi = \frac{1}{0.89k}, \quad \Gamma = \ln(\chi), \quad \Lambda = \beta k^2 \Gamma, \quad D = \Lambda + 2.$$

To derive and compute our results for $K^* \to \infty$, we divided each term by K^* and then we set $1/K^* > 0$. Thus the form of the eqn for $K^* \to \infty$, will contain only K^* terms of eqn (6), other terms will vanish. As $K^* \to \infty$, the dispersion relation is given by

$$\omega^2+\left[3\nu^*+\frac{2iv_b}{k}\right]\omega+k^2\left[\frac{k^2-1}{2}+\frac{E_b^2D}{4\pi\Lambda}+4\pi\sigma_b^2+\frac{2i\sigma_bE_b}{k\sqrt{\beta}}\left(\frac{1}{\Gamma}-2\right)\right]+3\nu^*ik^3v_b-k^2v_b^2=0. \quad (10)$$

3. Results and Discussion

The dispersion relation (6) which presents the temporal behavior of the system is investigated for several parameters. For all our computational purpose, we use $\beta = 77$, Hohman et al. (2001A).

Our aim here is to present the positive real part and the imaginary part of the solution ω of the equation (6), which is called, respectively, the growth rate and the frequency of the unstable mode, and these contributes to our understanding of the temporal instability. From our computational results, it is observed that the positive real part of ω is independent of the basic state velocity v_b, only the imaginary part depends on v_b. All the parameters we choose yielded negative imaginary part for nonzero basic state velocity. We use JMSL library to compute the complex zeros of the (6) whose coefficients are complex. Method Compute Zeros of the class Zero Polynomial of JMSL is used.

Figure 2 through 4 present results for constant applied field and for various values of E_b. Here, we consider four values 0.0, 0.97, 1.93 and 2.9. Results in Figure 2 are for infinite conductivity case, i.e., $K^* = \infty$. Others are parameters chosen as $v_b = 1,\ \nu^* = 0, \sigma_b = 0$.

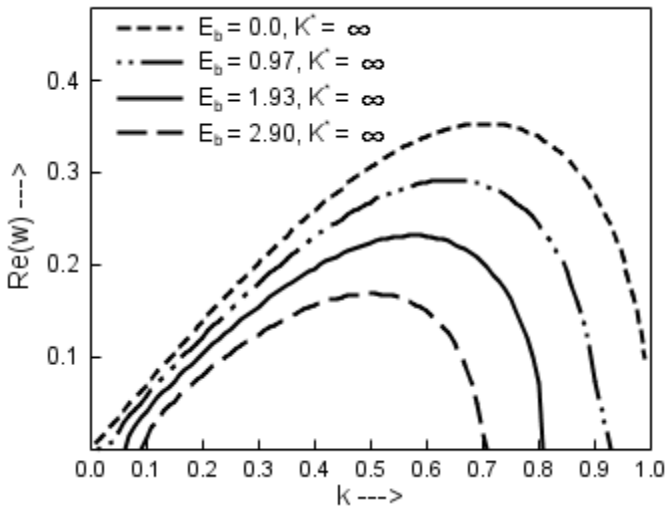

Figure 2. Positive real part of ω as a function *k* with

$K^* = \infty, \nu^* = 0, \sigma_b = \sigma_0 = 0$ and $v_b = v_0 = 1$ for various $E_b (= \Omega_0)$.

As can be seen from the Figure 2, the instability is reduced with increasing the magnitude of the applied field. The results indicate presence of the electrically analog of the so-called Rayleigh mode of instability, Drazin and Reid (1981). The results presented in the Figure 2 are also in

qualitative agreement with those reported in Hohman et al. (2001) for a perfect conducting fluid case and zero basic state velocity.

Results for zero conductivity, i.e., $(K^* = 0)$, and $K^* = 19.3$ cases are presented in Figure 3 and Figure 4, respectively, keeping other parameters same as in the Figure 2.

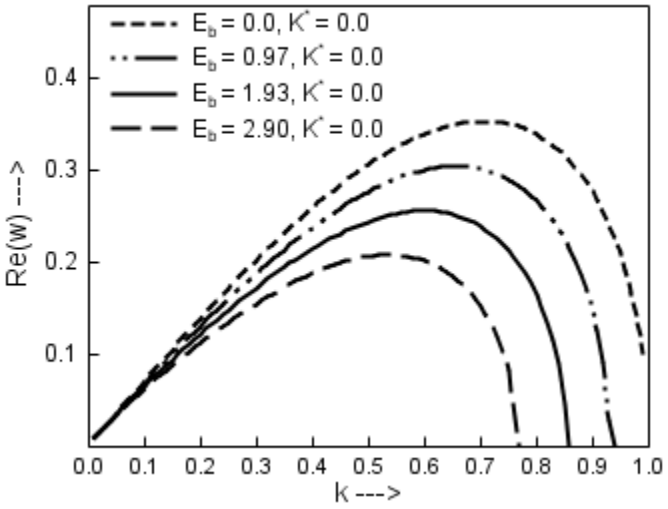

Figure 3. Positive real part of ω as a function k with $K^* = 0, \nu^* = 0, \sigma_b = 0$ and $v_b = 1$ for various E_b

As in the case of perfect conducting fluid, the results for the perfect dielectric fluid cases shown in the Figure 3 indicate that the flow instability is reduced with increasing the magnitude of the applied field, which is again a property of the Rayleigh type mode of jet instability. The results presented in the Figure 4 for a finite conducting case are qualitatively similar to those presented in the Figures 2-3 and indicate those results for Rayleigh type mode of instability.

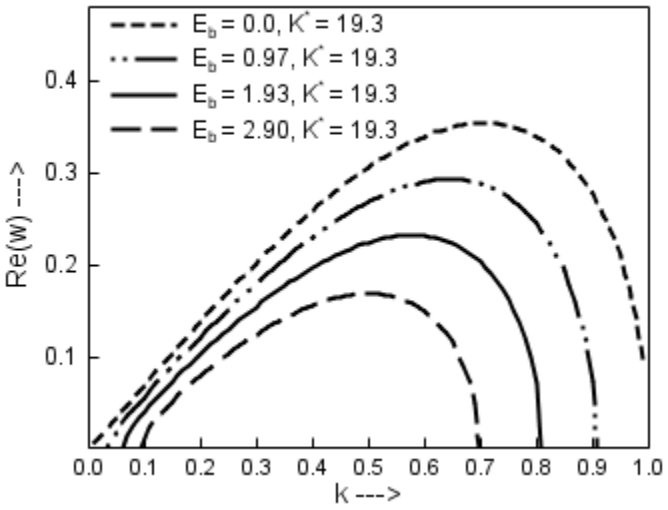

Figure 4. Positive real part of ω as a function k with $K^* = 19.3, \nu^* = 0, \sigma_b = 0$ and $v_b = 1$ for various E_b

Figure 5 presents some results for the constant applied field and compares the positive real solutions for three different conductivity cases, namely, zero, infinite and finite (19.3) for $E_b = 2.9, \nu^* = 0, \sigma_b = 0$ and $v_b = 1$. It is noticed that the results are closed to each other for $K^* = 19.3,$ and $K^* = \infty.$ It is seen from the Figure 5 the stability effect due to conductivity of the fluid.

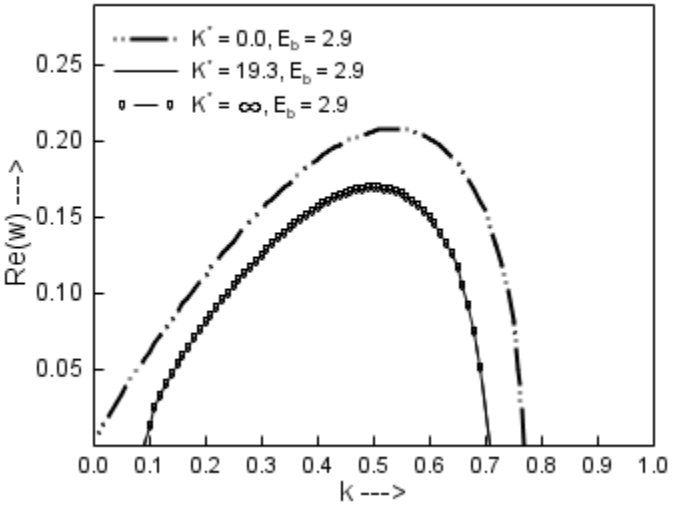

Figure 5. Positive real part of ω as a function k with $E_b = 2.9, \nu^* = 0, \sigma_b = 0$ and $v_b = 1$ for various K^*

The effect of ν^* is shown in Figure 6 for zero and finite conductivities. Other parameters used are $E_b = 2.9,\ \sigma_b = 0$ and $v_b = 1$. Again the case of constant applied field is considered here. It can be seen from the results presented in the Figure 6 that both viscosity and conductivity reduce the instability of the unstable mode.

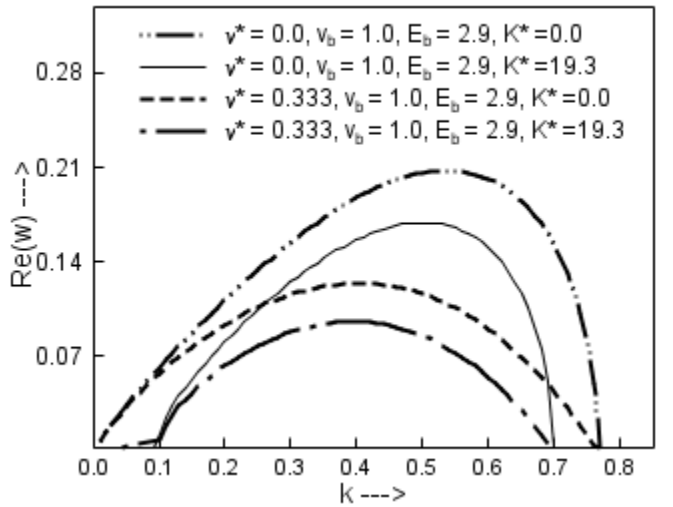

Figure 6. Positive real solutions of ω as a function k with $\sigma_b = 0$ and $v_b = 1$ for various ν^* and K^*

The effect of surface charge is presented next. Figure 7 displays the effect of σ_b for zero conductivity with $E_b = 2.9,\ \nu^* = 0$ and $v_b = 1$. It is seen from the results shown in the Figure 7 that surface charge density enhances the instability of the unstable mode for the axial wave number not too close to zero; while the opposite is true if the wave number is sufficiently small.

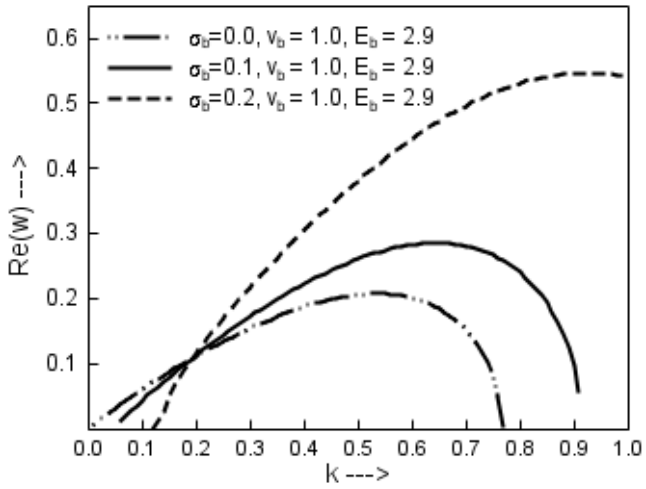

Figure 7. Positive real solutions of ω as a function k with $K^* = 0, \nu^* = 0, E_b = 2.9$ and $v_b = 1$ for various σ_b

Figure 8 presents results for variable applied field, finite and nonzero viscosity and conductivity and for different values of the strength of the applied field. It can be seen from the results shown in the Figure 8 that the instability mode favors intermediate values of the axial wave number (not too close to zero or one values).

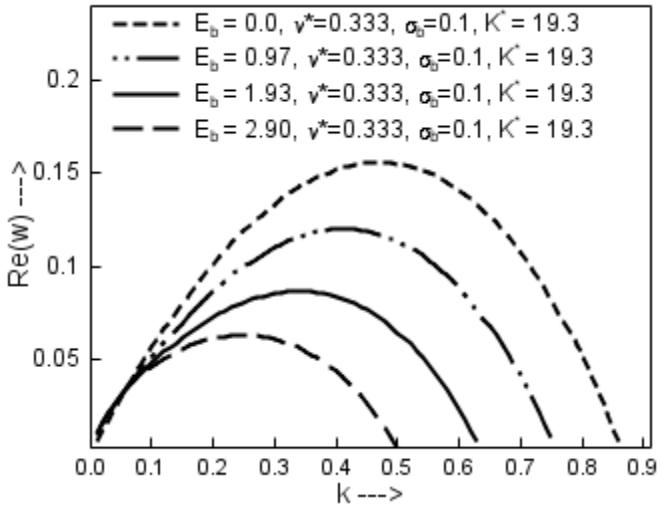

Figure 8. Positive real solutions of ω as a function k with $K^* = 19.3, \nu^* = 0.333, \sigma_b = 0.1$ and $v_b = 1$ for various E_b

It is observed from numerical investigations that there are two modes of instability for small values of *k*. The primary mode dominates the secondary mode. The secondary mode exists only for small values of *k*. The secondary mode is also independent of basic state velocity, i.e., real part of ω does not depend on the basic state velocity which is the case for primary mode also. The secondary modes are presented in Figure 9 with $K^* = 19.3, \nu^* = 0, \sigma_b = 0.1,\ v_b = 1$ for various E_b.

A comparison of these two modes are shown in Figure 10 for $K^* = 19.3, \nu^* = 0, \sigma_b = 0.1,\ v_b = 1$ and $E_b = 2.9$. For very small values of *k*, the secondary mode exists whereas for larger *k*, this mode does not exist. For larger values of *k*, only one mode (namely, primary mode) exists.

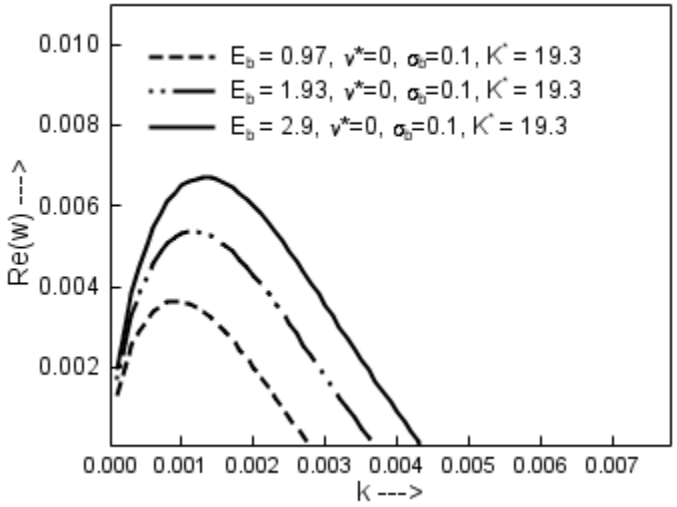

Figure 9. Secondary mode: positive real solutions of ω as a function *k* with $K^* = 19.3, \nu^* = 0, \sigma_b = 0.1,$ and $v_b = 1$ for various E_b

Figure 10. Primary and Second modes with $K^* = 19.3, \nu^* = 0, \sigma_b = 0.1,\ v_b = 1$ and $E_b = 2.9$

Figure 11 through Figure 13 presents the imaginary part of the frequency of the unstable mode versus the axial wave number for zero conductivity and finite conductivity. Other parameters varied are viscosity and basic state velocity. It can be seen from the Figure 11 that the period of the unstable mode is smaller for larger value of the basic state velocity and decreases with increasing the axial wave number of the unstable mode. Also, rate of increase of the frequency of the unstable mode with respect to the axial wave number increases with the basic state velocity.

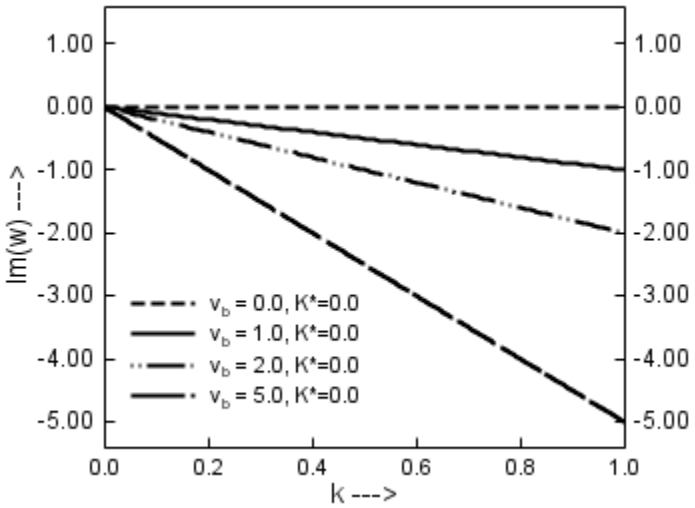

Figure 11. Imaginary part of ω whose real part is positive with $K^* = 0, \nu^* = 0, \sigma_b = 0.1, E_b = 2.9$

It can be seen from the Figure 12 that the imaginary part of ω of the unstable mode for finite conductivity and zero viscosity case has sudden change in magnitude when *k* is close to 0.68.

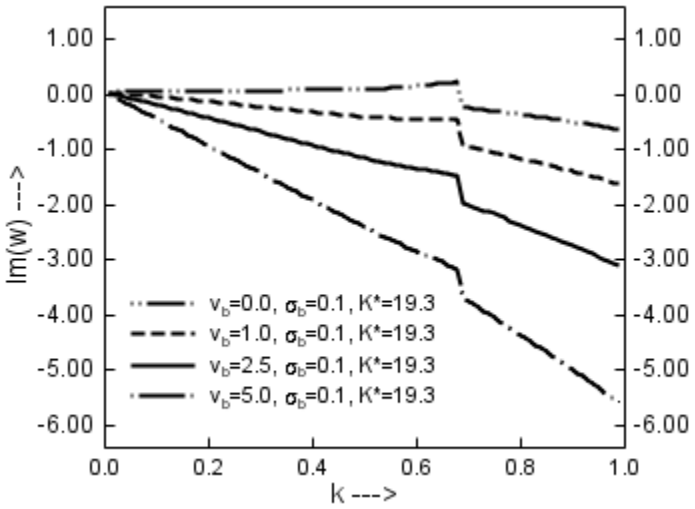

Figure 12. Imaginary part of ω whose real part is positive with $K^* = 19.3, \nu^* = 0.0, \sigma_b = 0.1, E_b = 2.9$

Figure 13 presents the results for imaginary part of ω with $K^* = 19.3, \nu^* = 0.333, \sigma_b = 0.1,$ and $E_b = 2.9$ for various basic state velocities. These is no unstable mode for k approximately bigger than 0.5.

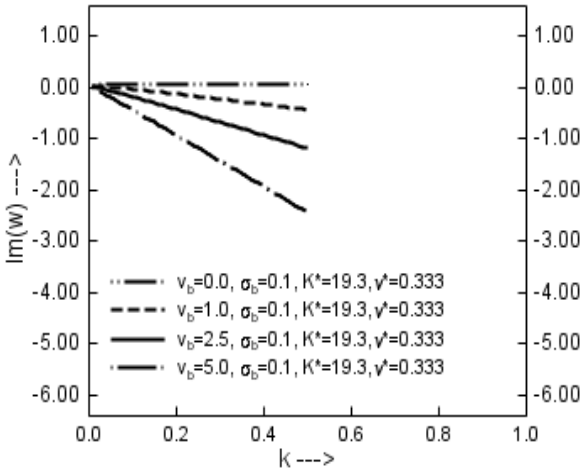

Figure 13. Imaginary part of ω whose real part is positive with $K^* = 19.3, \nu^* = 0.333, \sigma_b = 0.1, E_b = 2.9$

4. Conclusions

We conclude that in the realistic cases of the non-zero basic state velocity, the growth rate of the unstable mode is unaffected by the value of the basic state velocity. However, the non-zero value of the basic state velocity affects significantly the period of the unstable mode in the sense that it decreases the period, and the rate of increase of the frequency with respect to the axial wave number increases with the basic state velocity. In all the cases that we investigated we found that the presence of the variable applied field is destabilizing, while the finite values of either viscosity or conductivity are stabilizing. It is also noticed for the zero conductivity case that the imaginary part of ω is zero if basic state velocity is zero and the imaginary part of ω is nonzero if basic state velocity is nonzero. It is also observed from numerical investigations that there are two modes of instability for small values of the wavenumber. The primary mode dominates the secondary mode. The secondary mode exists only for small values of k. The secondary mode also independent of basic state velocity, i.e., real part of ω does not depend on the basic state velocity which is the case for primary mode also.

Acknowledgement

Authors would like to thank the referees for their constructive comments.

REFERENCES

Baily, A.G. (1988). Electro-Static Spraying of Liquid, Wiley, New York.

Drazin, P. G. and Reid, W. H. (1981). Hydrodynamic Stability, Cambridge University Press, UK.

Fridrikh, S. V., Yu J. H., Brenner, M. P. and Rutledge, G. C. (2003). Controlling the fiber diameter during electrospinning, Phys. Rev. Lett. **90,** 144502.

Hohman, M. M., Shin, M., Rutledge, G. and Brenner, M. P. (2001a). Electrospinning and electrically forced jets. I. Stability theory, Physics of Fluids **13** (8), 2201-2220.

Hohman, M. M., Shin, M., Rutledge, G., and Brenner, M. P. (2001b). Electrospinning and electrically forced jets. II. Applications, Physics of Fluids **13** (8), 2221-2236.

Li, D. and Xia, Y. (2004). Direct fabrication of composite and ceramic hollow nanofibers by electrospinning, Nano Lett. **4,** 933-938.

Melcher, J. R. and Taylor, G. I. (1969). Electro hydrodynamics: A review of the interfacial Shear stresses, Annu. Rev. Fluid Mech. **1,** 111-146.

Reneker, D. H., Yarin, A. L. and Fong, H. (2000). Bending instability of electrically charged liquid jets of polymer solutions in electrospinning, J. Appl. Phys. **87,** 4531-4547.

Riahi, D. N. (2009). On spatial instability of electrically forced axisymmetric jets with variable applied field, Appl. Math. Modelling, **33,** 3546-3552.

Saville, D. A. (1971). Electro hydrodynamic stability: effects of charge relaxation at the interface of a liquid jet, J. Fluid Mech. **48**(4), 815-827.

Shkadov, V. Y. and Shutov, A. A. (2001). Disintegration of a charged viscous jet in a high electric field, Fluid Dyn. Res. **28,** 23-39.

Sun, Z., Zussman, E., Yarin, A. L., Wendorff, J. H., and Greiner, A. (2003). Compound core-shell polymer nanofibers by co-electrospinning, Advanced Materials **15,** 1929-1932.

Yarin, A. L., Khoombongse, S., and Reneker, D. H. (2001). Bending instability in electrospinning of nanofibers, J. Appl. Phys. **89,** (2001) 3018-3026.

Yu, J. H., Fridrikh, S. V., and Rutledge, G. C. (2004). Production of sub micrometer diameter fibers by two-fluid electrospinning, Advanced Materials **16,** 1562-1566.